DOI: 10.1002/ejic.201001085

Density Functional Calculations on Protonation of the [FeFe]-Hydrogenase Model Complex $Fe_2(\mu\text{-pdt})(CO)_4(PMe_3)_2$ and Subsequent Isomerization Pathways

Caiping Liu,[a] Jamie N. T. Peck,[b] Joseph A. Wright,[b] Christopher J. Pickett,*[b] and Michael B. Hall*[a]

Keywords: [FeFe]-Hydrogenase / Protonation / Isomerization / Hydrides / Density functional calculations

Results of density functional theory (DFT) calculations on the protonation of the [FeFe]-hydrogenase model complex, $Fe_2(\mu\text{-pdt})(CO)_4(PMe_3)_2$ (pdt = propane-1,3-dithiolate), show that diiron bridging-hydride species are more stable than iron terminal-hydride, sulfur-hydride, or formyl isomers. Consistent with experimental observation, the *transoid* basal/basal forms are more stable than other μ-H isomers. With an ether as the proton carrier, $[Et_2OH]^+$, the favoured reaction pathways appear to involve weak coordination to CO followed by transfer of the proton from ether to an iron terminal site rather than directly to the bridging site. These kinetically favoured terminal-hydride species isomerize through a low-energy Ray-Dutt twist to produce the apical/basal bridging-hydride isomer. This isomer rearranges over somewhat higher barrier Bailar twists to the *cisoid* and *transoid* basal/basal isomers, the former finally rearranging to the latter isomer.

Introduction

Dihydrogen (H_2) is a promising clean energy carrier if simple and efficient methods of production, storage, and use can be developed. Inspired by the rapid and reversible H_2 oxidation and proton reduction catalyzed by the natural hydrogenase enzymes, considerable research has been devoted to design and synthesize species to mimic the active sites of the hydrogenases.[1] There are three main classes of hydrogenase in terms of the composition of the transition-metal-containing active site: [FeFe]-hydrogenase or Fe-only hydrogenase; [NiFe]-hydrogenase; and [Fe]-hydrogenases or Hmd.[1,2] The [NiFe]-hydrogenases are primarily utilized for H_2 oxidation, while the [FeFe]-hydrogenases are primarily utilized for H^+ reduction. Differently, the monoiron hydrogenases are utilized to activate dihydrogen in a catabolic process.

To understand the nature of hydrogen evolution at diiron sites and to explore the possibility of a synthetic catalyst, organometallic diiron complexes possessing key structural features of the active site of [FeFe]-hydrogenases have been intensively and widely explored.[1a,3–7] For the initial step in the hydrogen evolution at a multi-iron site, the proton can bind two Fe centers to form a bridging-hydride or a single Fe atom to form terminal-hydride.[3,8,9] It is also possible that the protonation can occur at sulfur or CO.[7b,10] Many experimental observations have shown that the bridging-hydride species is thermodynamically favoured.[3c,3d,4a,8,9,11] However, several studies suggest that at low temperature the terminal-protonation can be observed by NMR spectroscopy especially for the complexes possessing strong donor and chelating ligands, and that upon warming the terminal-hydrides isomerize to the bridging-hydrides.[5,9,11] Therefore, it is important to gain a better understanding of the protonation process.

Recently, Wright and Pickett reported a kinetic study on the protonation of a subsite analogue of [FeFe]-hydrogenase: $Fe_2(\mu\text{-pdt})(CO)_4(PMe_3)_2$.[3c] They proposed a two-step mechanism: (1) protonation of the apical-basal isomer; (2) rearrangement to the *trans*-basal isomer (Scheme 1).[3c] Later, using time-resolved NMR, stopped-flow UV and IR, Pickett and co-workers explored a series of similar diiron subsite models.[3d] Their observations were consistent with direct protonation at the bridging site followed by the isomerization for complexes containing two PMe_3 ligands, while for complexes with cyanide, the protonation occurred at cyanide followed by migration to the bridging site. They did not observe protonation at a single Fe to form the terminal-hydride.[3d]

Using density functional theory (DFT) calculations, we studied the mechanisms for the protonation of $Fe_2(\mu\text{-pdt})(CO)_4(PMe_3)_2$.[3c–3d] Because the formation of a terminal-hydride, which appears to be responsible for the H_2

[a] Department of Chemistry, Texas A&M University, College Station, Texas 77843-3255, USA
Fax: +1-979-845-6077
E-mail: hall@chem.tamu.edu
[b] Energy Materials Laboratory, School of Chemistry, University of East Anglia, Norwich, NR4 7TJ, UK
Supporting information for this article is available on the WWW under http://dx.doi.org/10.1002/ejic.201001085.

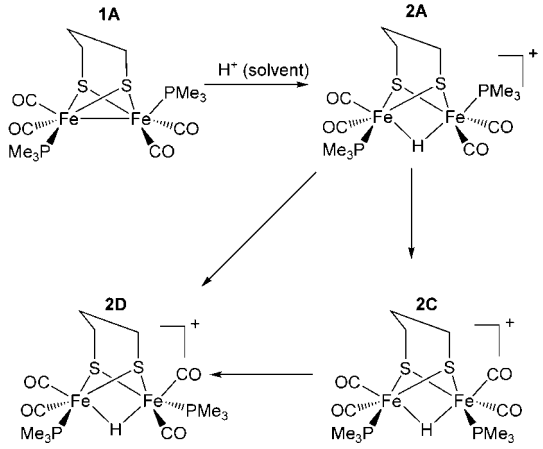

Scheme 1. Wright–Pickett proposed mechanism (ref.[3c]).

evolution in the enzyme[1b,12] could also be applicable to the synthetic systems,[4a,5e,9a,9d] many researchers have explored the possibilities of the formation of terminal-hydrides. Recent theoretical studies have shown that the activation barriers for formation of terminal-hydrides were lower than or close to those of the bridging-hydrides.[13,14]

Results and Discussion

Due to the numerous isomers, the computational models are classified into four isomeric types (**A**, **B**, **C**, and **D**) according to the relative position of the PMe_3 ligands (Scheme 2). Reaction of **1** with $HBF_4{\cdot}Et_2O$ in MeCN may proceed to four different kinds of hydrides (**2**, **3**, **4**, and **5**). Unless otherwise noted, all calculated energies presented in the text and figures are the solvent corrected free energies in kcal/mol.

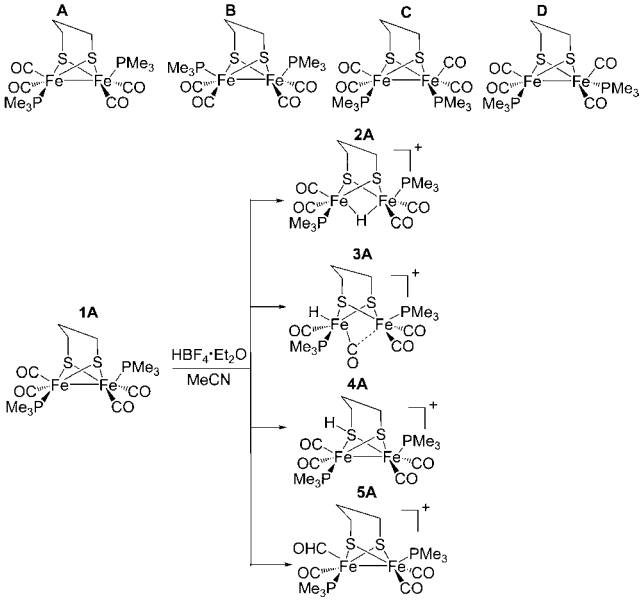

Scheme 2. Model complex $Fe_2(\mu\text{-pdt})(CO)_4(PMe_3)_2$ isomers and possible resulting hydrides.

Isomers of $Fe_2(\mu\text{-pdt})(CO)_4(PMe_3)_2$ and $[HFe_2(\mu\text{-pdt})(CO)_4(PMe_3)_2]^+$

The Unprotonated Isomers

The DFT-optimized structure of the unprotonated $Fe_2(\mu\text{-pdt})(CO)_4(PMe_3)_2$ **1D** isomer reproduces well the molecular structure derived from the X-ray crystallography (see Table S1).[4a] In the solid state, this complex adopts the basal/basal *transoid* (**1D**) geometry, while the apical/basal (**1A**) arrangement is dominant in solution.[3c] The calculated results agreed well with the experimental observation.[3c,4a] In the gas phase, isomers **1A** and **1A′** are 1.2 and 0.9 kcal/mol less stable than **1D**. Under the influence of solvent, the free energy of all the isomers spans a smaller range and **1A** and **1B** are stabilized relative to **1D**, respectively.

Isomer **1A** is now the most stable, as observed in the experiments. It should be noted that the calculations predict that the isomers with the largest dipole moments **1B** and **1C** are more strongly stabilized by the solvation corrections. Isomer **1B** is now the second most stable isomer, although its free energy is only 0.1 kcal/mol lower than **1D**, a difference far less that the accuracy expected from DFT calculations. Although other functionals raise the relative energy of this isomer, we believe that much of this very small error originates in the solvent correction (see Table S3). All the calculations agree that isomer **1C** is the least stable and interestingly it also has the longest Fe–Fe bond among these species. As shown in Figure 1, the "flip" of the pdt bridge (i.e. alternating direction of bridgehead carbon in the propane S–to–S linker) has little effect on the free energy of **1A**. Interconversion of these isomers by rotation of a $Fe(CO)_2(PMe_3)$ unit occurs through barriers ranging from 4 to 11 kcal/mol, while "flipping" the bridging propane dithiolate has a barrier of 9.4 kcal/mol (see Table S4).

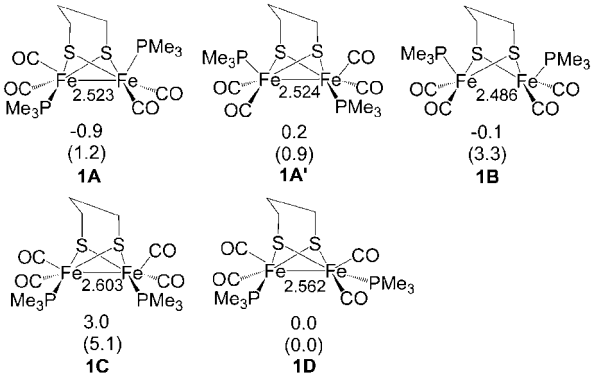

Figure 1. Relative solvent corrected free energies for isomers of $Fe_2(\mu\text{-pdt})(CO)_4(PMe_3)_2$, including **A′** the isomer with a "flipped" pdt bridge. The gas-phase electronic energies are reported in parentheses. Energies are given in kcal/mol, and the distances shown are in Å.

Bridging-Hydride Isomers

Protonation at 10 °C of $Fe_2(\mu\text{-pdt})(CO)_4(PMe_3)_2$ by $HBF_4{\cdot}Et_2O$ in MeCN was observed to yield a mixture of three isomeric bridging-hydrides by their NMR spectra.[3c]

Like the unprotonated species, there are four unique phosphane positional isomers, and the presence of the bridging hydride increases the energy difference between them (Figure 2). The basal/basal *transoid* (**2D**) geometry is stable by a sufficiently large margin that one would expect the other isomers to transform to **2D** at higher temperature.[13b] The deviation of the calculated bond lengths of **2D** from the X-ray crystallographic data[4a] is found to be less than 0.068 Å (see Table S2). As compared with the **1** series, protonation elongates the Fe–Fe bond to a similar distance for all the isomers. The Fe–H bond length is also similar in the isomers and averages 1.665 Å. In addition, the "flipped" isomer **2A′** is 1.9 kcal/mol less stable than **2A**, and the free energy barrier for the "flipping" the pdt linker is now only 4.2 kcal/mol (see Table S4).

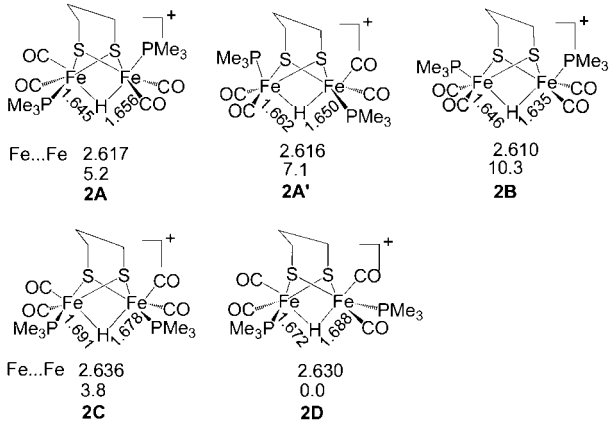

Figure 2. Relative solvent corrected free energies for four bridging-hydride isomers of $[(\mu\text{-H})Fe_2(\mu\text{-pdt})(CO)_4(PMe_3)_2]^+$, including isomers with "flipped" pdt bridge (labeled by prime). Energies are given in kcal/mol, and the distances of Fe···Fe and Fe–H are given in Å.

Terminal-Hydride Isomers

At low temperature, the proton can bind to a single iron atom, a result which has been reported by several groups.[5b,5c,9a,9d,11c] For the model of $[FeHFe(\mu\text{-pdt})(CO)_4(PMe_3)_2]^+$, the calculations provide eighteen unique isomers as listed in Figure 3.

Binding a proton terminally transforms that Fe into a face-bridged octahedral geometry, while the other Fe keeps its square pyramidal geometry. Since phosphanes do not appear at bridging sites, all these isomers have one terminal CO group in a semi-bridging position. The semi-bridging CO is always closer to the protonated Fe by 0.5 to 0.8 Å. The most stable structures still correspond to the basal/basal *transoid* isomers, in which **3D2** is about 1.0 kcal/mol less stable than **3D1**. On average, the **A**, **B**, **C**, and **D** terminal-hydrides are 17.8, 19.4, 17.6 and 18.4 kcal/mol higher, respectively, than the corresponding bridging-hydrides. Thus, in this system the terminal-hydrides could act as intermediates in the formation of the bridging-hydrides, but might be difficult to stabilize.

The position of hydride also has an effect on relative stabilities of these isomers. For the apical/basal species, the

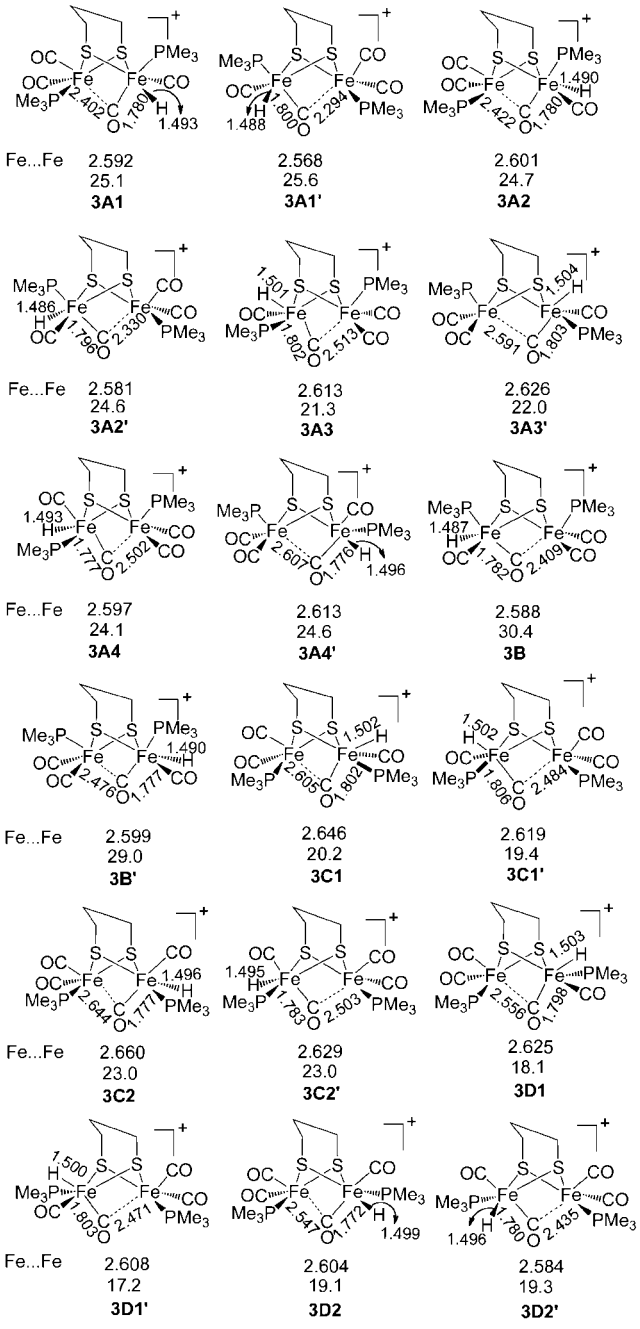

Figure 3. Relative solvent corrected free energies for the terminal-hydride isomers of $[FeHFe(\mu\text{-pdt})(CO)_4(PMe_3)_2]^+$, including isomers with "flipped" pdt bridge (labeled by prime). Energies are relative to the most stable isomer of $[(\mu\text{-H})Fe_2(\mu\text{-pdt})(CO)_4(PMe_3)_2]^+$ (**2D**) from Figure 2, and are given in kcal/mol, and the distances of Fe···Fe, Fe–CO and Fe–H are shown in Å.

isomers with the hydride at the apical position are found to be more stable than corresponding conformers with the basal hydride. Like the aforementioned **1** and **2** series, "flipping" the pdt linker has little influence on the energy of the terminal-hydride isomers (Figure 3). For example, the isomers **3A1′**, **3A2′**, **3A3′**, and **3A4′** are only 0.5, 0.1, 0.7 and 0.5 kcal/mol less stable than their corresponding "unflipped" isomers, indicating these isomers could coexistent

during the protonation process. In comparison with the bridging-hydride isomers, the Fe–Fe bonds in the terminal-hydrides are generally shorter, but still longer than those of the unprotonated species, while the Fe–H bond lengths are shortened by 0.17 Å on average.

Sulfur-Protonated Isomers

Alternatively, protonation could occur at one of sulfur atoms of the dithiolate linker (μ-$SCH_2CH_2CH_2S$) to form the thiolate complex, $\{(\mu\text{-}SCH_2CH_2CH_2SH)[Fe_2(CO)_4(PMe_3)_2]\}^+$. Figure 4 shows eight possible isomers. The isomers have similar stabilities except for the two *cisoid* basal/basal isomers, **4C1** and **4C2**, whose relative free energies are higher than the others but similar to each other. Here, the apical/apical isomer **4B** is found to be the most stable in solution, its free energy is 0.2, 0.4, and 1.4 kcal/mol lower than **4A1**, **4A2**, and **4D**, respectively. The calculated free energy in solution of **4B** is 29.4 and 10.3 kcal/mol higher than those of the bridging hydride **2D** and the terminal hydride **3D2**, respectively. Thus, protonated S species will be difficult to generate. Again, the alternative arrangement of the pdt linker produces isomers with slightly higher energy.

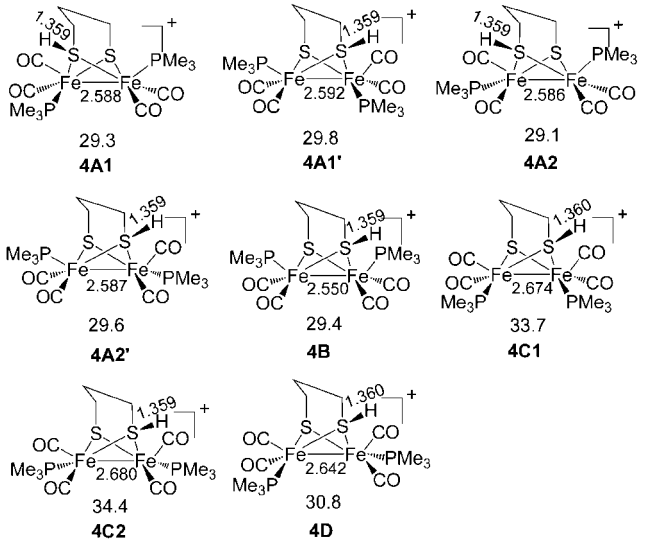

Figure 4. Relative solvent corrected free energies for the sulfur-protonated isomers of $\{(\mu\text{-}SCH_2CH_2CH_2SH)[Fe_2(CO)_4(PMe_3)_2]\}^+$, including isomers with "flipped" pdt bridge (labeled by prime). Energies are relative to the most stable isomer of $[(\mu\text{-}H)Fe_2(\mu\text{-pdt})(CO)_4(PMe_3)_2]^+$ (**2D**) from Figure 2, and are given in kcal/mol, and the distances shown are in Å.

CO-Protonated Isomers

As mentioned by Best and Pickett, it is possible for a CO ligand to be protonated to form the formyl species.[7b] Our calculations find one class of formyl isomers maintains the Fe–Fe bond length with an average length of about 2.66 Å, which is longer than the mean values of the aforementioned hydrides, and one terminal CO group is transferred to the semi-bridging position. However, these isomers are among those of the highest energy. When the terminal CO group at the basal position is protonated, as shown in **5A3**, **5B1**, and **5B2**, the distance between this CO group and iron is lengthened and the energy is even higher. A second class of isomers have the Fe–Fe bond broken and formation of a four-member ring, composed of two Fe atoms and C=O. As shown in Figure 5, the distance between two iron atoms averages 3.145 Å, and the Fe···O distance averages about 2.051 Å. Although the second class of isomers presents species with free energies slightly lower than the S-protonated species, these formyl species may be difficult to generate because Fe–Fe bond breaking will likely lead to a significant barrier. Formyl species of the first class may be kinetically accessible, but they are among the least stable protonated species (note that reduction of the system will stabilize these formyl species[15]).

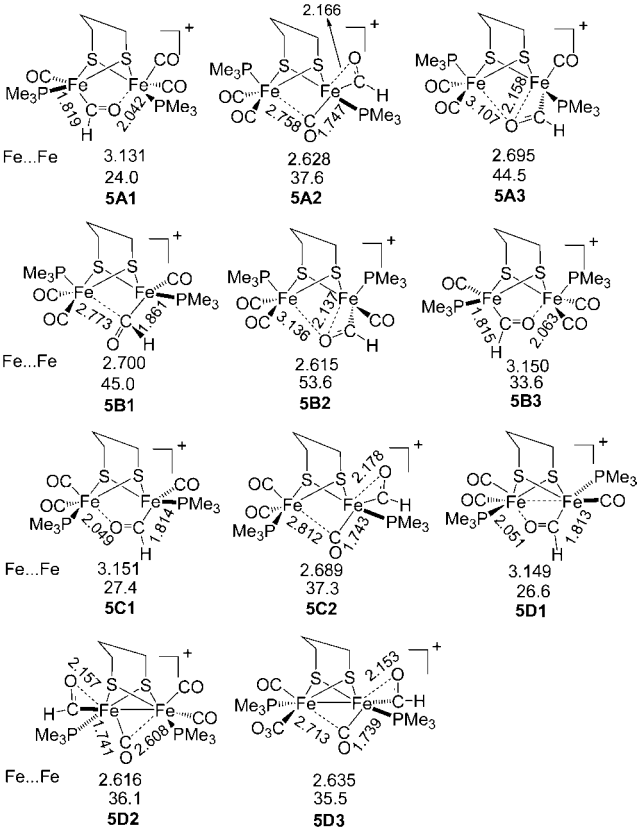

Figure 5. Relative solvent corrected free energies for the CO-hydride isomers of $[Fe_2(\mu\text{-pdt})(CHO)(CO)_3(PMe_3)_2]^+$. Energies are relative to the most stable isomer of $[(\mu\text{-}H)Fe_2(\mu\text{-pdt})(CO)_4(PMe_3)_2]^+$ (**2D**) from Figure 2, and are given in kcal/mol, and the distances shown are in Å.

According to the above results, protonation of either sulfur or CO generates significantly higher energy species than bridging- and terminal-hydrides. Therefore, only mechanisms that avoid the formation of these high-energy species are discussed below. The transition states (TS) are identified by having one and only one imaginary frequency. The intermediates connected to these TS were determined by following the intrinsic reaction coordinate (IRC) both forward and backward (see Computational details). The pdt ligand "flips" back and forth easily, and the two isomers are generally very close in energy. In the following sections we have

not profiled all the paths for both isomers, but as we will show the key steps are independent of this "flipping" motion.

Ether-Mediated Protonation Directly to Bridging-Hydrides

As reported by De Gioia, Schollhammer and their coworkers,[13] the solvent might be involved in the protonation processes. We examined both $[Et_2OH]^+$ and $[CH_3CNH]^+$ as proton carriers and found that the former is more stable in free energy (see Table S6). Although an equilibrium may exist between these two solvated species, the free energy difference suggests that $[Et_2OH]^+$ will dominate even though the concentration of CH_3CN is higher than that of Et_2O. As $[Et_2OH]^+$ approaches the complex, it first appears to coordinate weakly to CO and then the proton transfers via two possible pathways to produce the final bridging-hydride product (Scheme 3): (1) the bridging-path, where the proton transfers directly from $[Et_2OH]^+$ to the bridging position and (2) the terminal-path, where the proton transfers from $[Et_2OH]^+$ to the terminal position forming a species that then rearranges to more stable bridging-hydride species. These two protonation paths will be described in the next two sections.

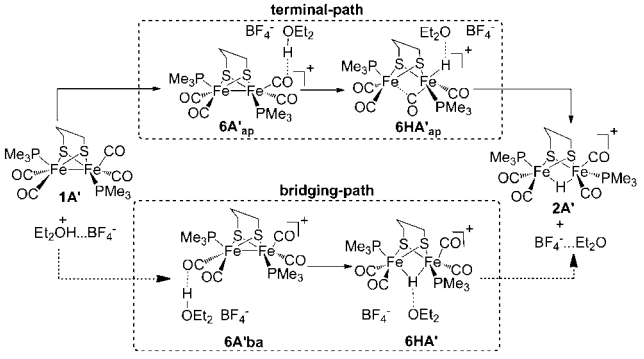

Scheme 3. Possible ether-mediated mechanisms: terminal-path and bridging-path.

Figures 6, 7, and 8 show the potential-energy profiles and geometric structures of key intermediates and transition states for the formation of the bridging-hydride isomers **2A**, **2C**, and **2D**, respectively. The results for **2B**, the computationally least stable and experimentally unobserved isomer, are presented in Figure S1 and Figure S3 (see Supporting Information). Some of the key structures are also shown in the Figures. The diiron complex plus the ion pair ($[Et_2OH]^+\cdots[BF_4]^-$) are taken as the starting point and the protonated isomer plus the ether-ion pair ($Et_2O\cdots[BF_4]^-$) are taken for the product in the following proposed mechanisms mainly to preserve the number of species in the reaction. Alternative choices will simply scale the initial and final energy (left most and right most columns of the Figures) with respect to the rest of the energies. According to the IRC calculations the transition states for the H^+ transfer leads back to an intermediate with $[Et_2OH]^+$ coordinated to a terminal CO at the basal position and forward to an intermediate with the Et_2O weakly coordinated to the Fe bound hydride.

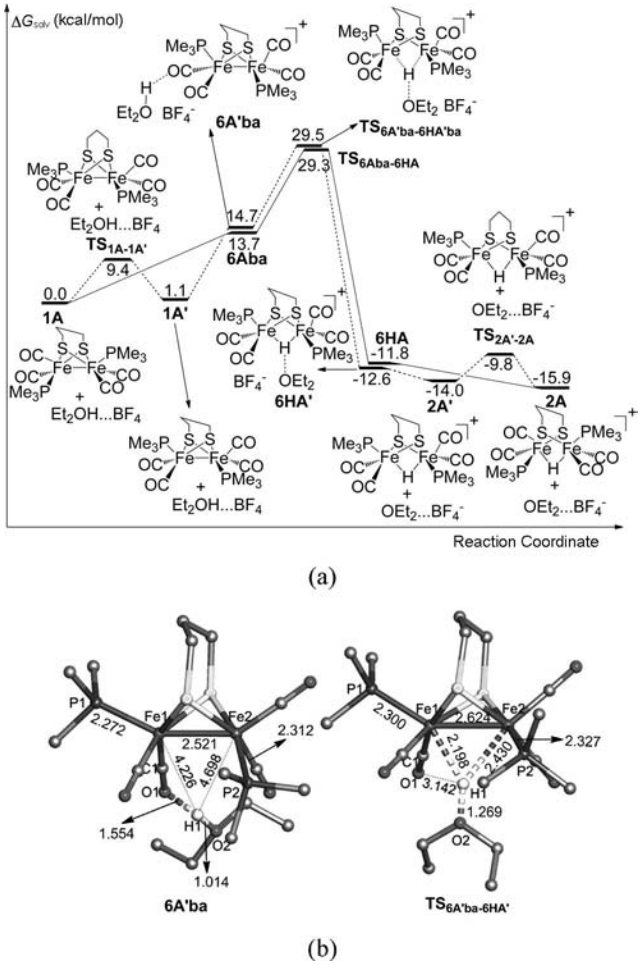

Figure 6. (a) Energy profile for the bridging-path of the ether-mediated mechanism for the formation of **2A**, the relative free energies are given in kcal/mol, and the structures with bridge-flipped analogues (**6Aba**, $\mathbf{TS_{6Aba\text{-}6HA}}$, and **6HA**) are not shown; (b) optimized structures for the ether-mediated intermediate and transition state, the hydrogen atoms of the PMe_3 groups and ether are omitted for the sake of clarity and the bond lengths are given in Å.

Formation of **2A** (Figure 6) proceeds from the intermediate **6A′ba**, which is stabilized by the hydrogen interaction between proton and CO, to $\mathbf{TS_{6A'ba\text{–}6HA'}}$, which transfers the proton to generate the bridging hydride at a free energy barrier of 14.8 kcal/mol from **6A′ba**. In this TS, the H moves close to the iron atoms (≈ 2.3 Å) and the O–H bond lengthens by 0.25 Å. The initial product, **6HA′**, has a weak "H-bond" between Et_2O and the hydride; coordination of ether to $[BF_4]^-$ generates the product, **2A′** (loss of ether to the solvent may be more likely but this procedure preserves the number of species in the reaction). During this proton transfer process the PMe_3 ligands maintain their apical/basal positions. Attack of $[Et_2OH]^+$ at the Fe–Fe bond leads to the expansion bridging structure, the Fe–Fe lengthens and the ligands on both irons tip away from the newly forming hydride ligand (comparing $\mathbf{TS_{6A'ba\text{–}6HA'}}$ with **6A′ba**

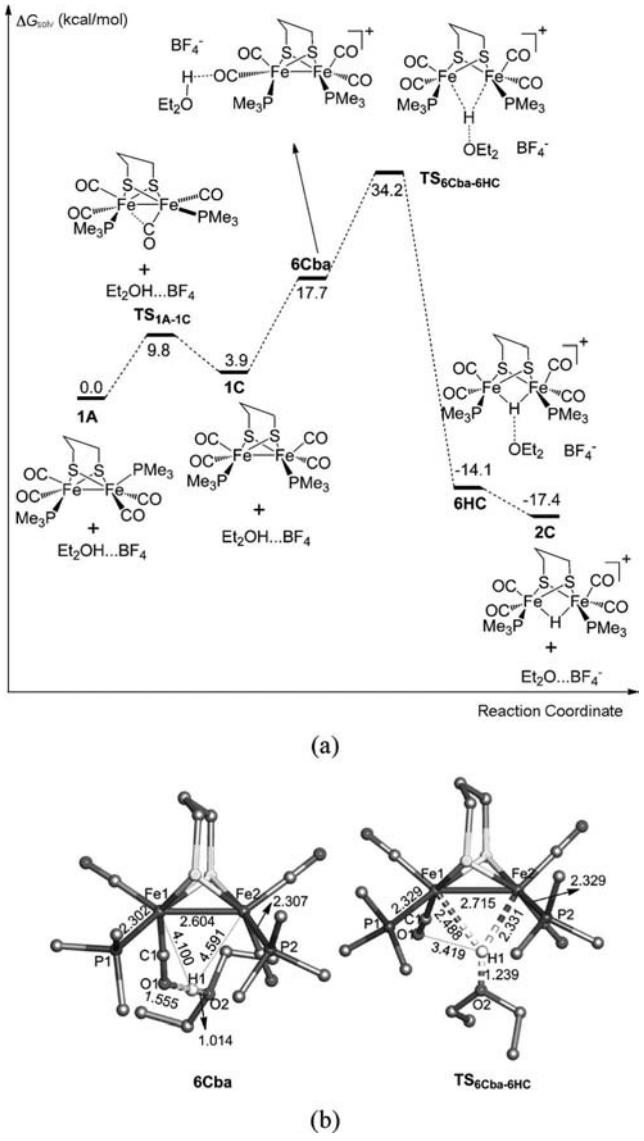

Figure 7. (a) Energy profile for the bridging-path of the ether-mediated mechanism for the formation of **2C**, the relative free energies are given in kcal/mol; (b) Optimized structures for the ether-mediated intermediate and transition state, the hydrogen atoms of the PMe_3 groups and ether are omitted for the sake of clarity and the bond lengths are given in Å.

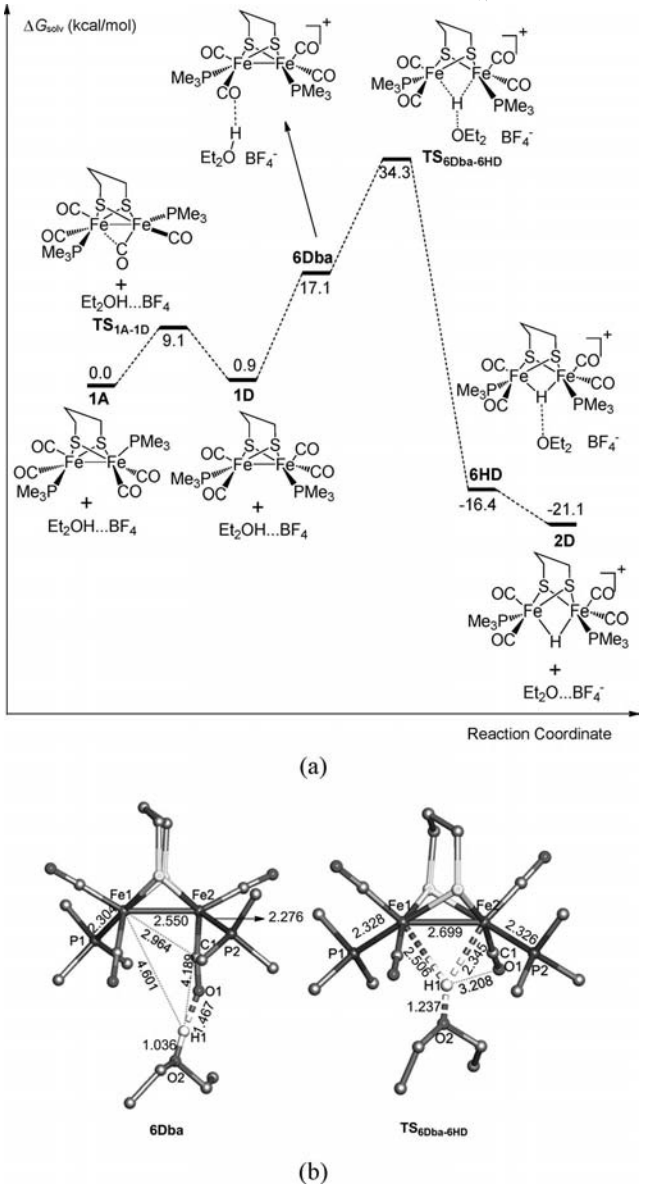

Figure 8. (a) Energy profile for the bridging-path of the ether-mediated mechanism for the formation of **2D**, the relative free energies are given in kcal/mol; (b) Optimized structures for the ether-mediated intermediate and transition state, the hydrogen atoms of the PMe_3 groups and ether are omitted for the sake of clarity and the bond lengths are given in Å.

the Fe2···C1 lengthens by 0.420 Å, and the C1–Fe–Fe2–P2 dihedral angle enlarges by 23.1°). As shown in Figure 6a, the "flip" of the pdt linker has little effect on the calculated results; further, the intermediates and transition state **6Aba**, **6HA** and $\mathbf{TS_{6Aba–6HA}}$ show similar geometric parameters (see Figure S3). Another possible pathway is the attack of $[Et_2OH]^+$ to the basal CO group located opposite to both the bridgehead carbon in pdt linker and the apical PMe_3 ligand, the relative free energy barrier via transition state $\mathbf{TS_{7A'ba–7HA'}}$ is found to be only 1.2 kcal/mol lower than the barrier through $\mathbf{TS_{6A'ba–6HA'}}$ (see Figure S2). And the intermediate reactant and product (**7A′ba** and **7HA′ba**) are 1.4 and 0.5 more stable than **6A′ba** and **6HA′ba**, respectively. These results indicate that the influence of the positions of the PMe_3 ligands is small.

Figure 7 shows the two steps that are involved in the formation of **2C**. Firstly, **1A** rotates to give **1C** via the low-energy transition state $\mathbf{TS_{1A–1C}}$, then $[Et_2OH]^+$ attacks **1C** to form **6Cba**. Transfer of H occurs through transition state $\mathbf{TS_{6Cba–6HC}}$, which is 4.7 kcal/mol higher than $\mathbf{TS_{6A'ba–6HA'}}$ even though the final product **2C** of this reaction is 1.4 kcal/mol more stable than **2A**.

The most stable product, **2D**, can be generated (Figure 8) by following a pathway similar to **2C**. Although the product **2D** is 3.8 kcal/mol more stable than **2C**, the barriers along these two paths are similar. The structure of the intermediate **6Dba** is interesting as the $[Et_2OH]^+$ coordinated CO

group moves to the semi-bridging position with a Fe1···C1 distance that is 0.26 and 0.20 Å shorter than those in **6A′ba** and **6Cba** (Fe2···C1), respectively.

The relative free-energy barriers for the formation of the product, **2**, from the same starting point, either **1A** plus $[Et_2OH]^+$, or the H-bonded precursor **6**, are lowest for **2A**, and higher for both **2C** and **2D**. Thus, this bridging-path mechanism favours the initial formation of **2A**, which could then be followed by rearrangements to the more stable **2C** and **2D**. Although this mechanism appears consistent with the experimental results, the calculations predict lower energy paths for other mechanisms (vide infra).

Protonation Directly to Terminal-Hydrides

As shown in Scheme 3 an alternative mechanism can be developed that involves $[Et_2OH]^+$ attacking the CO group in a manner that leads to the formation of terminal-hydrides (i.e. the terminal-path). The coordination of $[Et_2OH]^+$ to apical and basal CO groups will lead to the corresponding apical- and basal-hydrides, respectively. These alternative mechanisms will be described below. In both cases the formation of a semi-bridging carbonyl species occurs synchronously with protonation; i.e. there is no distinct formation of an accessible site prior to proton transfer. Implicit in the current interpretation of the active site of the [FeFe]-hydrogenase is the availability of a vacant site for proton attack. In the case here, the "rotated state" is a transition state not a stable intermediate. Of course, if the system were such that the geometry was stable in the "rotated state", as expected for the enzyme, the barrier would be low.

Mechanism with 1A (1A′) as the Initial Reactant

As shown in Figure 9 (a), the coordination of $[Et_2OH]^+$ to the apical CO of **1A′** forms the intermediate **6A′ap**, then the proton transfers to a single iron atom to give the terminal-hydride intermediate **6HA′ap**. Both the absolute free-energy barriers from **1** and relative free-energy barriers from **6** for the H^+ transfer are found to be 1.9 and 1.6 kcal/mol lower than the barriers on bridging-path to **2A′**, respectively. Thus, formation of the terminal-hydride **3A3′** is kinetically favoured. In addition, the ether-coordinated intermediates **6** show similar hydrogen-bonding interactions to those on the bridging-path, see Figure 9 (b). Relative to **6A′ba** in bridging-path, the intermediate **6A′ap** has a slightly stronger H-bond.

Alternatively, the $[Et_2OH]^+$ can coordinate to the basal CO group to form the basal terminal hydride. Although the overall barrier from the neutral complex **1A′** is the same on this route, the weaker H-bond in **8A′ba** compared to that in **6A′ap** reduces the relative barrier by 4.0 kcal/mol in comparison with that in the apical-hydride formation, compare Figure 9 (a) and Figure 10 (a). The structure of these two H-bonded species differ in the position of the partially protonated CO, which is more semibridging in **8A′ba**.

The third possible coordination pattern similar to that through **7A′ba** is also considered, namely, $[Et_2OH]^+$ attacking the basal CO group located opposite to both the bridgehead carbon in pdt linker and the apical PMe_3 ligand to form the basal terminal hydride **3A4′** (see Figure 11). Here, the position of the PMe_3 ligand has a significant influence on the energy barrier. The overall barrier from the neutral complex **1A** is lowered 7.7 and 7.8 kcal/mol in comparison with the pathways shown in parts a of Figures 9 and 10, respectively. Moreover, the relative free energy barrier between the intermediate reactant (**9A′ba**) and transition state ($\mathbf{TS_{9A'ba–9HA'ba}}$) is only 4.5 kcal/mol, which is 8.7 and 4.7 kcal/mol lower than those between **6A′ap** and $\mathbf{TS_{6A'ba–6HA'ap}}$ and between **8A′ba** and $\mathbf{TS_{8A'ba–8HA'ba}}$, respectively. Thus, the formation of the terminal hydride

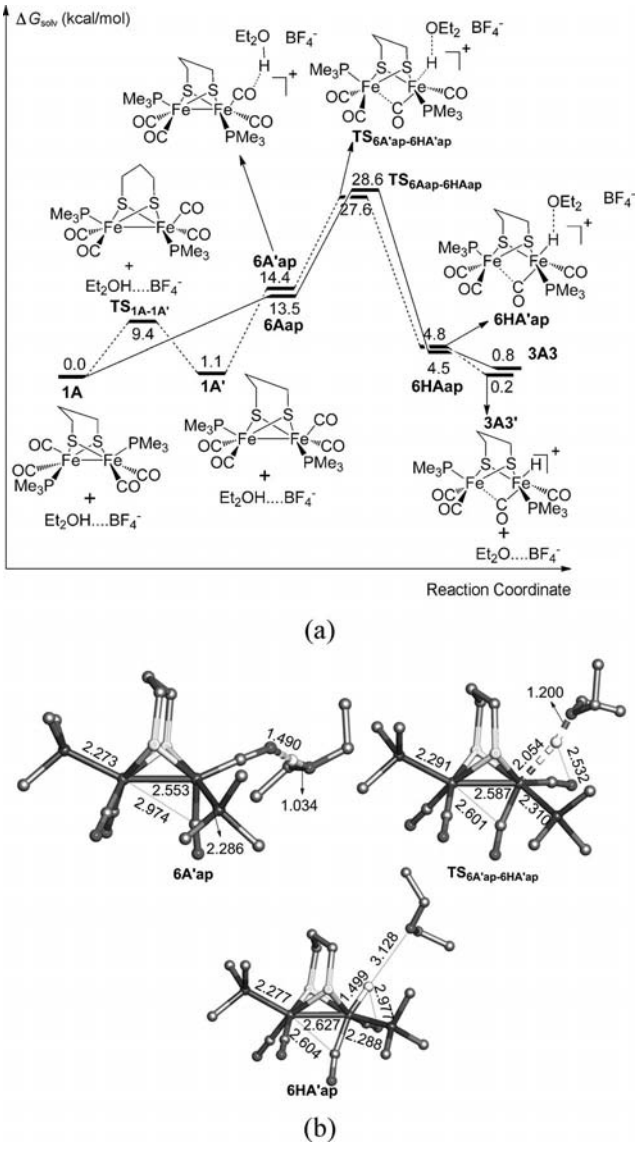

Figure 9. (a) Energy profile for the terminal-path of the ether-mediated mechanism for the formation of terminal-hydride isomer **3A3′**, the structures with bridge-flipped analogues (**6Aap**, $\mathbf{TS_{6Aap-6HAap}}$, **6HAap** and **3A3**) are not shown; (b) optimized structures for the intermediates and transition state. The hydrogen atoms of the PMe_3 groups and ether are omitted for the sake of clarity and the bond lengths are given in Å.

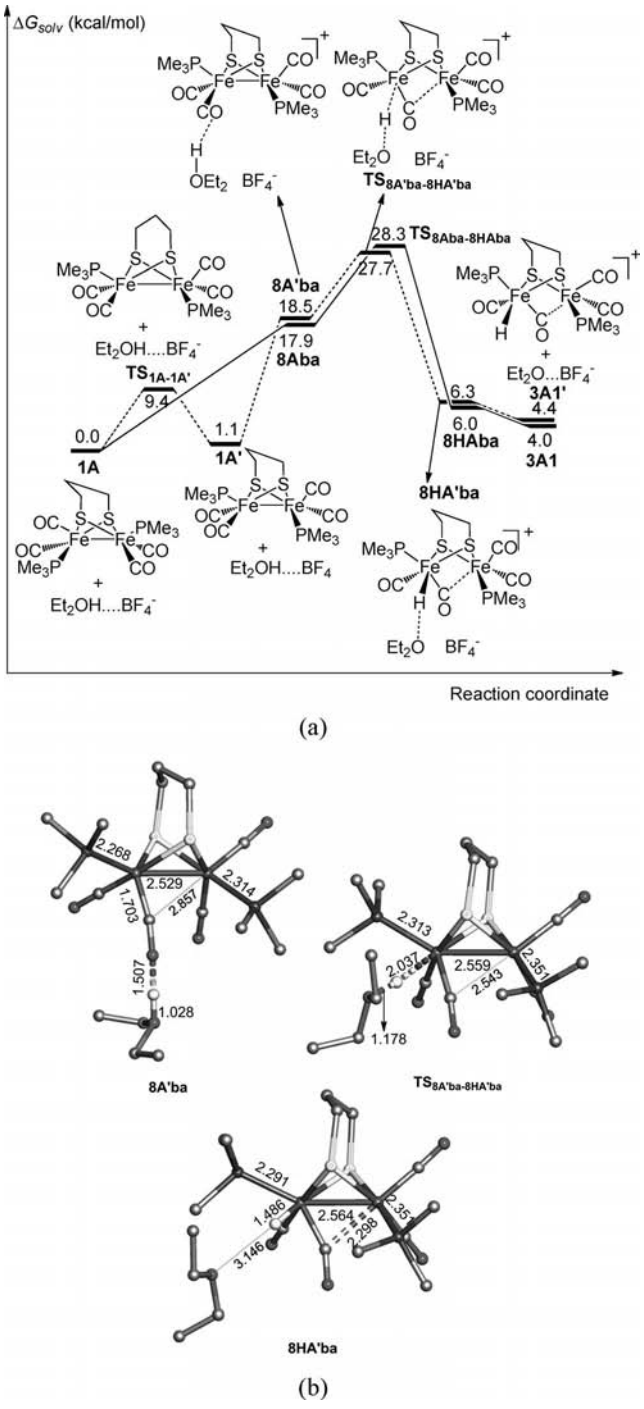

Figure 10. (a) Energy profile for the terminal-path of the ether-mediated mechanism for the formation of terminal-hydride isomer **3A1′**; (b) optimized structures for the intermediates and transition state. The hydrogen atoms of the PMe_3 groups and ether are omitted for the sake of clarity and the bond lengths are given in Å.

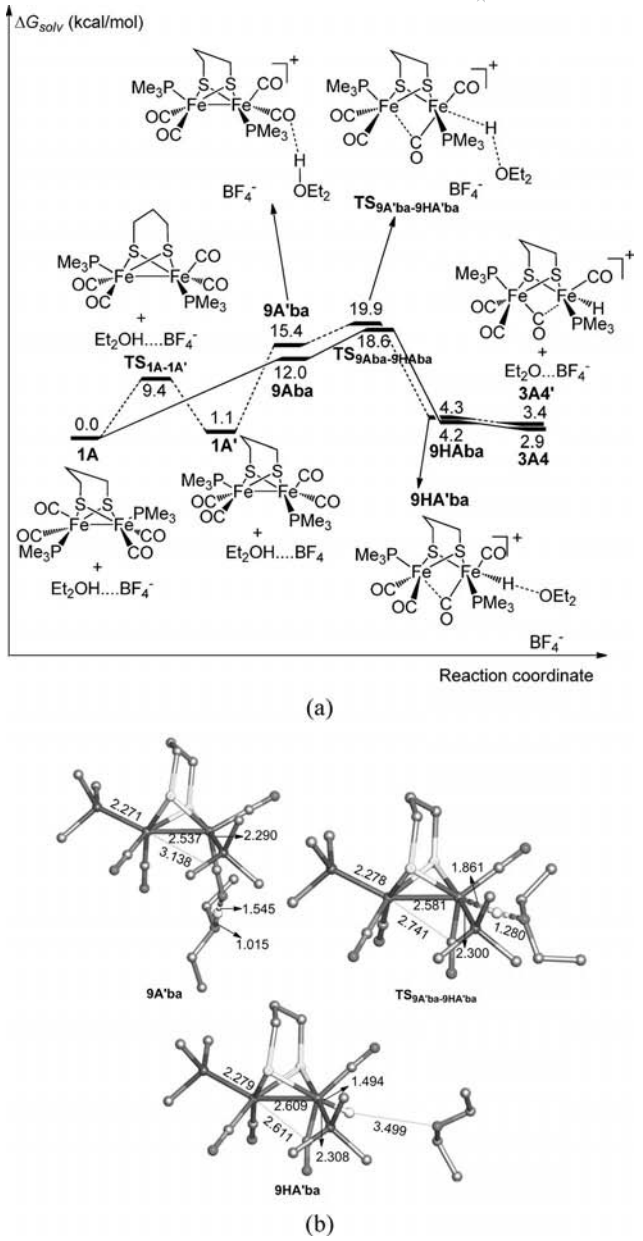

Figure 11. (a) Energy profile for the terminal-path of the ether-mediated mechanism for the formation of terminal-hydride isomer **3A4′**; (b) optimized structures for the intermediates and transition state. The hydrogen atoms of the PMe_3 groups and ether are omitted for the sake of clarity; bond lengths are given in Å.

3A4′ is kinetically preferred to **3A3′** and **3A1′**. Compared with the structures of **8A′ba**, $\mathbf{TS_{8A'ba–8HA'ba}}$, and **8HA′ba**, a less semibridging character can be found in **9A′ba**, $\mathbf{TS_{9A'ba–9HA'ba}}$, and **9HA′ba**, in which the bond length between the carbon atom of the attacked CO group and iron are lengthened about 0.281, 0.198 and 0.313 Å, respectively.

Mechanism with 1C as the Initial Precursor

Because the unprotonated **1A** is rapidly isomerizing to **1C** and **1D**, the ether-coordinated intermediates with two PMe_3 ligands either *transoid* or *cisoid* to each other need to be considered. Figure 12 (a) plots the energy profiles of the pathways via the *cisoid* terminal-hydride. Coordination of $[Et_2OH]^+$ to the apical CO group of **1C** forms the intermediate **6Cap**, and then the proton transfer takes place via a transition state with the energy barrier of 9.6 kcal/mol above **6Cap** to generate the apical-hydride **3C1′** via **6HCap**. In comparison with the path via **6A′ap** [Figure 9 (a)], the

free energy barriers relative to **1A** and **6** are lower by 1.2 and 3.6 kcal/mol, respectively, but not as low as the path via **9Aba**, see Figure 11 (a).

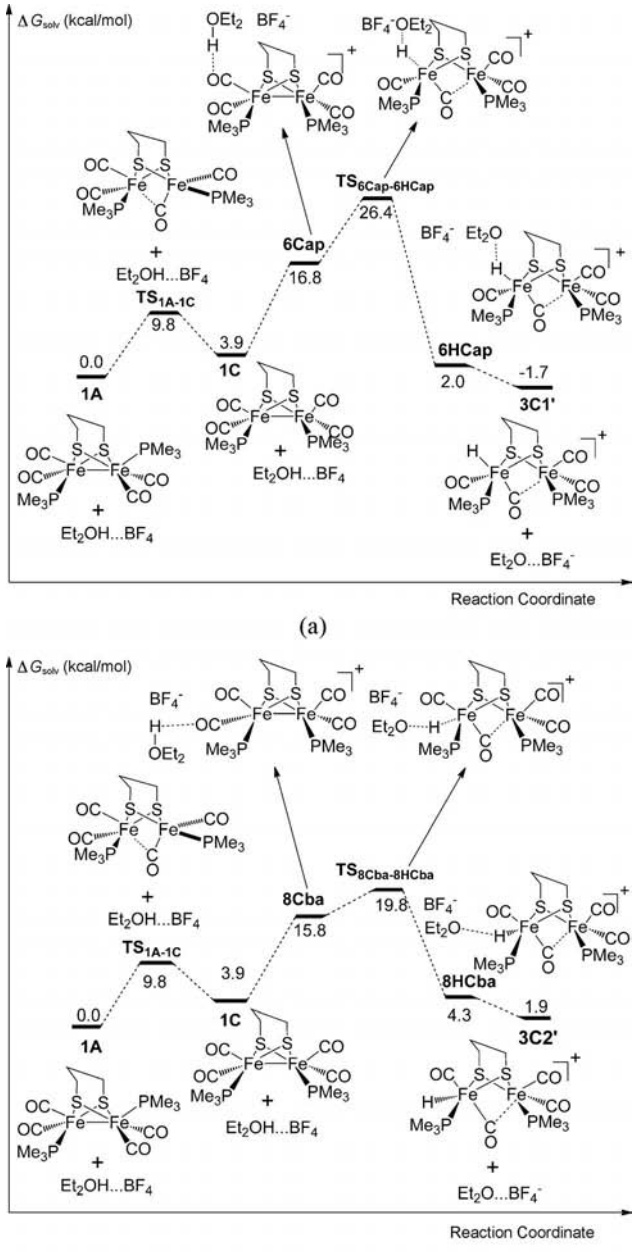

Figure 12. Energy profile for the terminal-path of the ether-mediated mechanism: (a) formation of terminal-hydride isomer **3C1′**; (b) formation of terminal-hydride isomer **3C2′**.

An unexpectedly low barrier is found for the formation of the terminal-hydride isomer **3C2′**. As shown in Figure 12 (b), $[Et_2OH]^+$ attack on the basal CO in **1C** (*cisoid*) results in $\mathbf{TS_{8Cba–8HCba}}$ that is 6.6 kcal/mol lower in free energy than $\mathbf{TS_{6Cap–6HCap}}$ [Figure 12 (a)]. In addition, this transition state $\mathbf{TS_{8Cba–8HCba}}$ is lowered in both absolute and relative free energy compared to $\mathbf{TS_{8A′ba–8HA′ba}}$ by 7.9 and 5.2 kcal/mol, respectively. This result indicates that $[Et_2OH]^+$ coordination at the basal position of the *cisoid* arrangement can avoid the high proton transfer barrier and easily generate a terminal-hydride. Comparing Figures 11 (a) and 12 (b), one can note similar energy barriers for these two pathways, indicating that the probabilities to form **3A4′** and **3C2′** are similar, while **3A4** is slightly favoured.

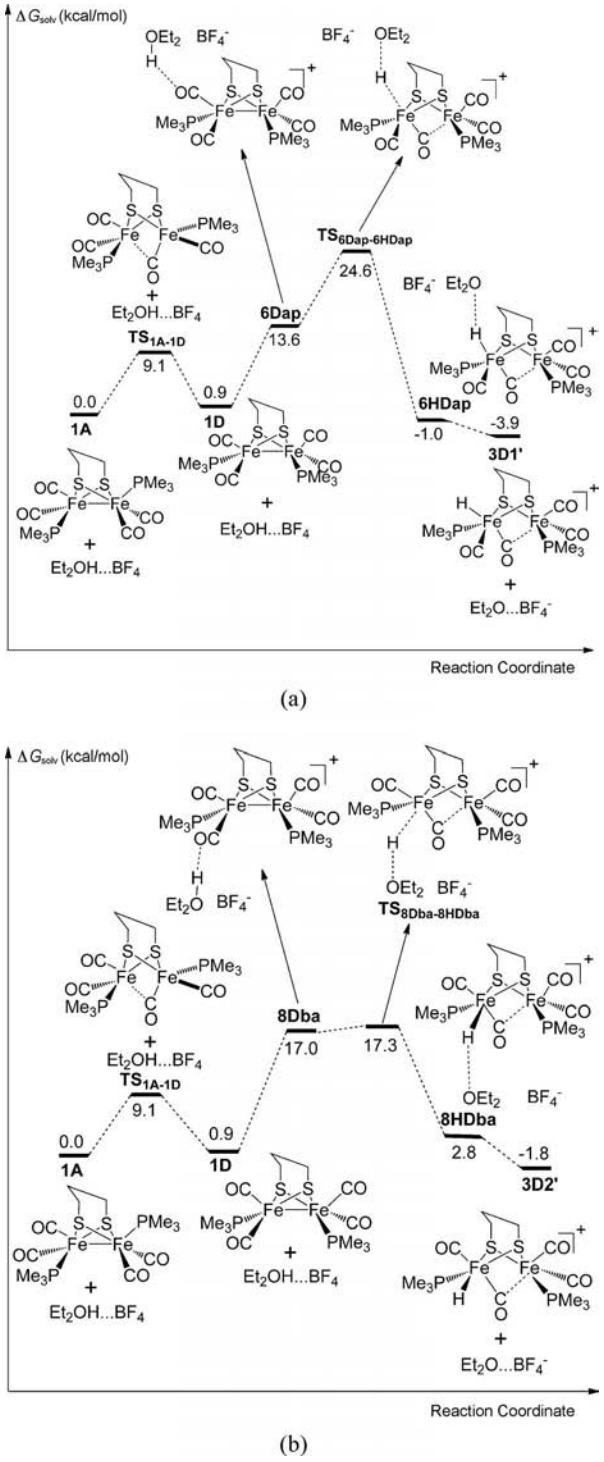

Figure 13. Energy profile for the terminal-path of the ether-mediated mechanism: (a) formation of terminal-hydride isomer **3D1′**; (b) formation of terminal-hydride isomer **3D2′**.

Mechanism with 1D as the Initial Precursor

Figure 13, shows that the *transoid* arrangement of the PMe_3 ligands produces pathways similar to those reported for the *cisoid* arrangement, but with even lower barriers for $[Et_2OH]^+$ attack on both apical and basal CO ligands. Again, the relative order of the barriers is similar. Thus, attack on the basal CO produces $\mathbf{TS_{8Dba–8HDba}}$, which is only 17.3 kcal/mol above **1A**, a barrier that is 2.5 kcal/mol below the lowest energy TS in the *cisoid* path, see Figure 12 (b) and 1.3 kcal/mol below the lowest energy TS in the apical-basal path, Figure 11 (a). In *transoid* case, the H-bonded intermediate is very weakly bound leading to a very small relative barrier between **8Dba** and $\mathbf{TS_{8Dba–8HDba}}$ of 0.3 kcal/mol.

As discussed above, the ether-mediated terminal-path mechanisms with attack of $[Et_2OH]^+$ on the basal CO group *cis* to a basal PMe_3 ligand to form terminal-hydrides (**3A4′**, **3C2′** and **3D2′**) are more favourable than direct attack to form the more stable bridging isomers. Furthermore, these pathways are also more favourable than the direct attack on the apical CO group or basal CO *cis* to an apical PMe_3 ligand in the formation of the terminal-hydrides of **3A3′**, **3A1′**, **3C1′** and **3D1′**. In the following sections we will examine the rearrangements from the terminal-hydride isomers to the bridging-hydride isomers and rearrangements among the bridging isomers.

Rearrangements from Terminal to Bridging Hydrides

Rearrangement from the Terminal-Hydrides 3A3′ and 3A1′

As shown in Figure 14 (a), the isomerization from the apical terminal-hydride to bridging-hydrides will need more than one step. Beginning at **3A3′**, there are three pathways to generate the bridging-hydrides **2A′** and **2B**. (1) Plotted as the solid line in Figure 14 (a); the three ligands: hydride, basal PMe_3, and basal CO in **3A3′** move in a Bailar twist to form **3A4′**, with a free-energy barrier of 20.1 kcal/mol, then the hydride at the basal position either interchanges with the semi-bridging CO to form **2A′** or rotates again to generate **2B**. Unfortunately, the former formation path, namely, via the pairwise exchange to form **2A′** cannot to be found, while the rotation with four ligands (via a Ray-Dutt twist) in **3A4′** leads to **2B** via the transition state $\mathbf{TS_{3A4′–2B}}$ with a free energy barrier of 16.8 kcal/mol. (2) Plotted as the dashed line in Figure 14 (a); the four ligands in **3A3′**: hydride, basal PMe_3, basal CO and the μ-CO rotate to give intermediate **6A′Int**, which presents a configuration with the PMe_3 ligand lying nearly in the plane composed by the apical PMe_3 and CO ligands and two irons. Although **6A′Int** is 10.4 kcal/mol less stable than **3A4′**, this rotation decreases the free energy barrier by 1.5 kcal/mol. Next, **6A′Int** may undergo a further rotation with a very low barrier of 4.9 kcal/mol, again rearranging to **2A′**. This pathway is composed of two continuous Ray-Dutt twists. (3) Plotted as the hashed line in Figure 14 (a); the three ligands: hydride, basal PMe_3 and basal CO in **3A3′** rotate clockwise to generate **3B′**. The energy barrier of this transition state

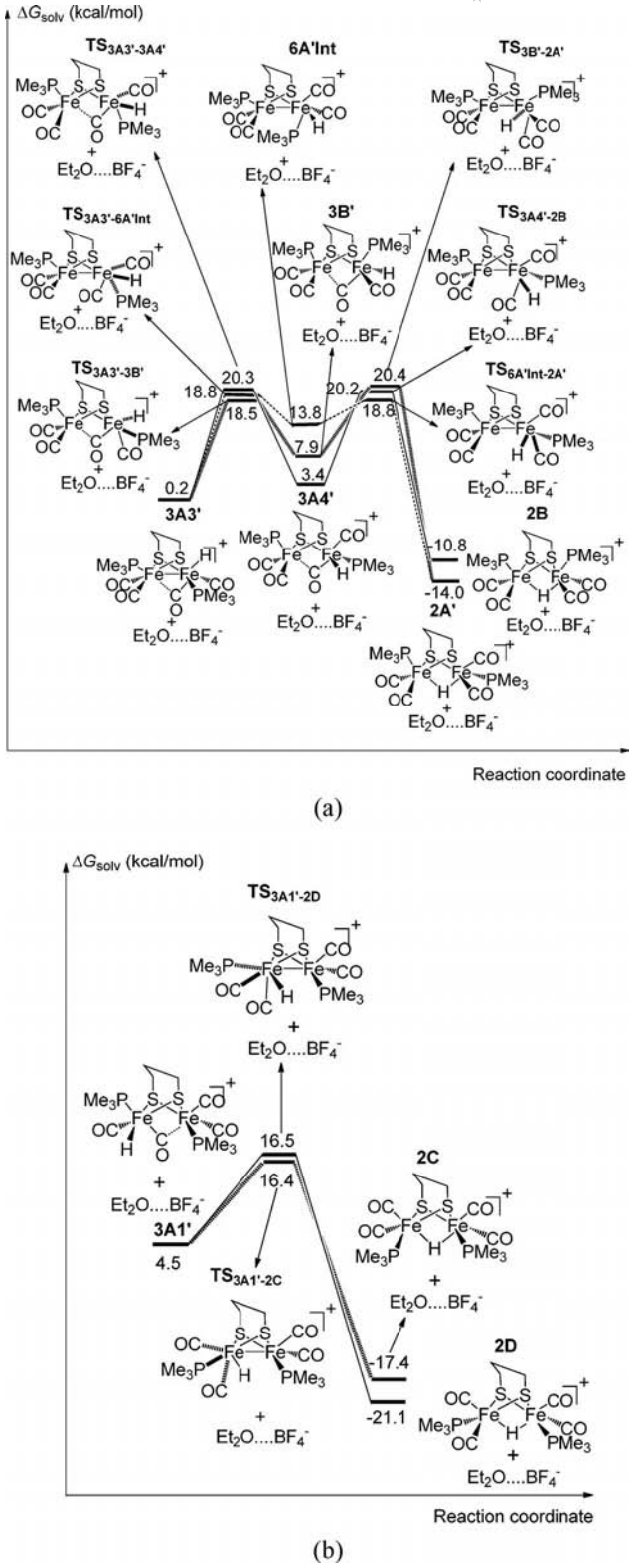

Figure 14. (a) Three pathways for the rearrangements from terminal-hydride **3A3′** to bridging-hydrides **2A′** and **2B**: solid line pathway: $\mathbf{3A3′ \rightarrow TS_{3A3′–3A4′} \rightarrow 3A4′ \rightarrow TS_{3A4′–2B} \rightarrow 2B}$; dashed line pathway: $\mathbf{3A3′ \rightarrow TS_{3A3′–6A′Int} \rightarrow 6A′Int \rightarrow TS_{6A′Int–2A′} \rightarrow 2A′}$; hashed line pathway: $\mathbf{3A3′ \rightarrow TS_{3A3′–3B′} \rightarrow 3B′ \rightarrow TS_{3B′–2A′} \rightarrow 2A′}$; (b) two pathways for the rearrangement from terminal-hydride **3A3** to bridging-hydrides **2C** and **2D**: solid line pathway: $\mathbf{3A1′ \rightarrow TS_{3A1′–2D} \rightarrow 2D}$; hashed line pathway: $\mathbf{3A1′ \rightarrow TS_{3A1′–2C} \rightarrow 2C}$.

$\mathbf{TS_{3A3–3B'}}$ is the lowest when compared with $\mathbf{TS_{3A3'–3A4'}}$ or $\mathbf{TS_{3A3'–6A'Int}}$, indicating that for the PMe_3 ligand the rotation from basal to apical is easier than from basal to basal. The next isomerization from **3B′** to **2A′** involves rotation of the four ligands with a barrier of 12.5 kcal/mol. This pathway is similar to the first one (**3A3′** → $\mathbf{TS_{3A3'–3A4'}}$ → **3A4′** → $\mathbf{TS_{3A4'–2B}}$ → **2B**), in which a Bailar twist is followed by a Ray-Dutt twist. As a whole, the overall free-energy barriers for these three rearrangements from terminal to bridging hydrides are very similar at 20.1, 18.6, and 20.2 kcal/mol, respectively.

The rearrangement from terminal hydride **3A1′** seems simple compared to the case of **3A3′**. Here, only one Ray-Dutt twist can generate the bridging-hydrides [see Figure 14 (b)]. Four ligands: basal hydride, basal CO, apical PMe_3 and μ-CO rotate clockwise to form **2D** and counter-clockwise to form **2C**, respectively. It is interesting that the two rotational transition states $\mathbf{TS_{3A1'–2D}}$ and $\mathbf{TS_{3A1'–2C}}$ are almost identical in energy, indicating that the probability to form **2C** and **2D** from **3A1′** are equal. This rearrangement from **3A1′** to **2C** and **2D** will be fast as the energy barrier is only 12 kcal/mol, an advantageous pathway in comparison with those presented in Figure 14 (a).

Rearrangement from Terminal-Hydrides of 3C1′ and 3C2′

Following three similar pathways for the rearrangement presented in Figure 15 (a), **3C1′** can rearrange to form **2A′** and **2D** as shown in Figure 15 (a). (1) Plotted as the solid line, the pathway via **3D2** shows a transition state $\mathbf{TS_{3C1'–3D2'}}$ with high energy barrier (29.0 kcal/mol). (2) Plotted as the dashed line, the path via **6CInt**, although better is still higher than 25 kcal/mol. (3) Plotted as the hashed line, the pathway via **3A2′** is more favourable, but its overall free energy barrier is 22.4 kcal/mol. Thus, the strong influence of the relative position of the two PMe_3 ligands makes all of these barriers high and hinders the rearrangement from **3C1′** to the bridging isomers.

Figure 15 (b) shows that the terminal hydride **3C2′** can be rotated directly to form **2A′** but with a free-energy barrier 4.6 kcal/mol higher than the pathway presented in Figure 14 (b).

Rearrangement from Terminal-Hydrides of 3D1′ and 3D2′

As shown in Figure 16 (a) the overall barriers to rearrange **3D1′** (apical hydride) to **2A′** or **2C** are 29.7 (solid line), 35.0 (dashed line) and 37.6 (hashed line) kcal/mol for the three possible pathways, respectively.

In contrast, the free-energy barrier for the rearrangement from the terminal hydride **3D2′** to **2A′**, see Figure 16 (b) is 18.4 kcal/mol, just 1.9 kcal/mol higher than the isomerization from **3C2′** to **2A′**, and even below the latter when compared to **1A**.

Clearly, the arrangement of the two PMe_3 ligands has a large effect on the energy barriers for the rearrangement from terminal to bridging hydrides. In the case of terminal hydrides with the hydride at the apical position, the barriers for the rotation of hydride from apical to basal position are found to increase dramatically when two PMe_3 ligands are located at the *cisoid* or *transoid* position. Although this trend can also be found in the case of terminal hydrides with the hydride at the basal position, the absolute free en-

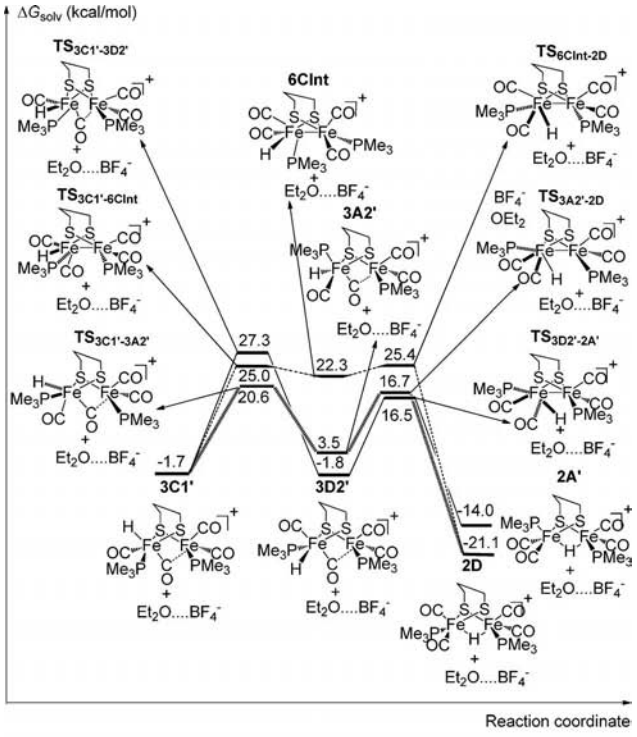

Figure 15. (a) Three pathways for the rearrangements from terminal-hydride **3C1′** to bridging-hydrides **2A′** and **2D**: solid line pathway: **3C1′** → $\mathbf{TS_{3C1'–3D2'}}$ → **3D2′** → $\mathbf{TS_{3D2'–2A'}}$ → **2A′**; dashed line pathway: **3C1′** → $\mathbf{TS_{3C1'–6CInt}}$ → **6CInt** → $\mathbf{TS_{6CInt–2D}}$ → **2D**; hashed line pathway: **3C1′** → $\mathbf{TS_{3C1'–3A2}}$ → **3A2′** → $\mathbf{TS_{3A2'–2D}}$ → **2D**; (b) pathway for the rearrangement from terminal-hydride **3C2′** to bridging-hydrides **2A′**: **3C2′** → $\mathbf{TS_{3C2'–2A'}}$ → **2A′**.

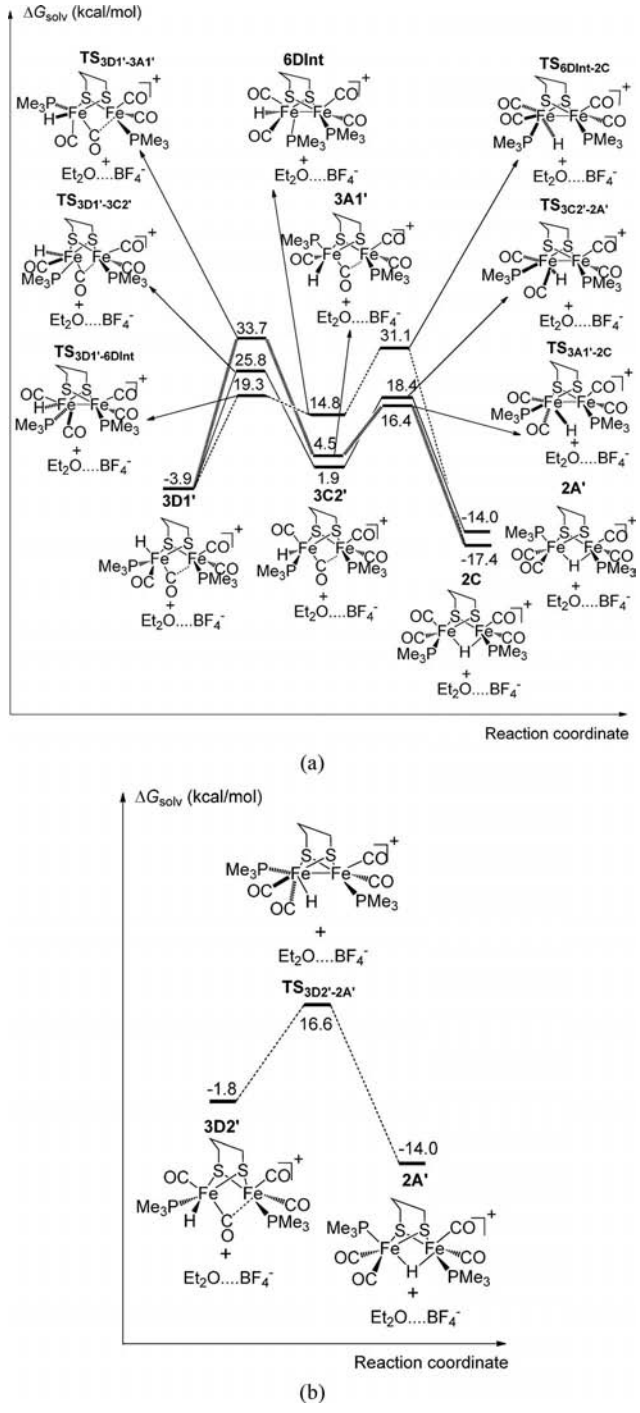

Figure 16. (a) Three pathways for the rearrangements from terminal-hydride **3D1′** to bridging-hydrides **2A′** and **2C**: (1) solid line pathway: **3D1′** → **TS$_{3D1'-3C2'}$** → **3C2′** → **TS$_{3C2'-2A'}$** → **2A′**; (2) dashed line pathway: **3D1′** → **TS$_{3D1'-6DInt}$** → **6DInt** → **TS$_{6DInt-2C}$** → **2C**; (3) hashed line pathway: **3D1′** → **TS$_{3D1'-3A1'}$** → **3A1′** → **TS$_{3A1'-2C}$** → **2C**; (b) pathway for the rearrangement from terminal-hydride **3D2′** to bridging-hydrides **2A′**: **3D2′** → **TS$_{3D2'-2A'}$** → **2A′**.

ergy barriers for these rearrangements to form the bridging isomers are as low as 15 to 17 kcal/mol. In combination with the formation of the terminal hydrides via **9A′ba**, **3A4′**, **8Cba**, **3C2′**, **8Dba**, and **3D2′** – see Figures 11 (a), 12 (b), 13 (b) – the more favourable rearrangements are via **TS$_{3A4'-2B}$**, **TS$_{3C2'-2A'}$** and **TS$_{3D2'-2A'}$** – see parts b in Figures 15, 16.

Rearrangements of Bridging-Hydrides

We also calculated the rearrangement between the bridging-hydrides (see Figure 17). The barriers to transition states **TS$_{2A'-2C}$**, **TS$_{2A'-2D}$** and **TS$_{2C-2D}$** are found to be slightly higher in free energy than TSs of the rearrangements from terminal hydrides to bridging hydrides presented in parts b of Figures 14, 15, and 16.

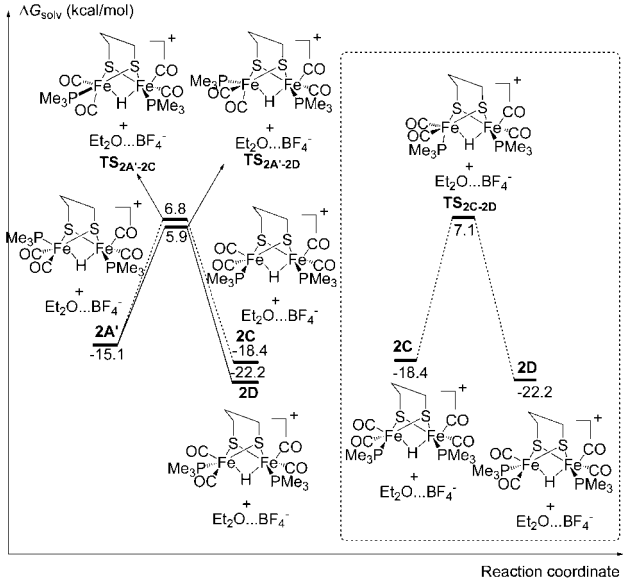

Figure 17. Energy profile for direct rotation between bridging-hydrides with "flipped" pdt bridge, the relative free energies are given in kcal/mol.

Conclusions

With the aid of the density functional theory (DFT) calculations, the possible protonated isomers and protonation mechanisms for the [FeFe]-hydrogenase model complex, $Fe_2(\mu\text{-pdt})(CO)_4(PMe_3)_2$, have been studied in detail. The calculations show that the isomers of the sulfur-hydrides and formyl species are much less stable than the bridging or terminal hydrides. Furthermore, for bridging and terminal hydrides, the *transoid* basal/basal forms are found to be thermodynamically more stable than other corresponding isomers. This prediction is consistent with the experimental observation for the bridging-hydride species.

In the exploration of the possible protonation process, our calculations reveal that the ether (or solvent) may play a role in the protonation process. With $[Et_2OH]^+$ as the proton carrier, the proton transfer pathways appear to involve an intermediate with $[Et_2OH]^+$ bound to a CO ligand followed by rearrangement to a terminal or bridging hydride. The lowest energy pathways involve formation of terminal

hydrides, rather than direct formation of the more stable bridging hydrides, the former then convert to bridging hydrides, which then interconvert between each other at a slower rate. Ignoring the "flip" of the pdt linker, the results show that there are three preferable pathways to form bridging-hydride via the terminal-hydrides **3A4**$^{(\prime)}$, **3C2**$^{(\prime)}$ and **3D2**$^{(\prime)}$ (see Figure S5), and the most favourable pathway is plotted in Scheme 4. Beginning with the rapid equilibrium between **1A** (the predominate species in some solvents) and **1D** (the apparently most stable crystalline form). Protonation of **1D** occurs preferentially as the barrier for protonation of **1A** is about 8 kcal/mol higher in free energy. The lowest energy path for protonation of **1D** produces **3D2′**, which rearranges rapidly to **2A′** through a Ray-Dutt twist, the species initially observed in the experiments. The species **2A′** then rearranges through Bailar twists on two paths **2A′**→**2D** (experimentally and computationally the faster route) and **2A′**→**2C**→**2D** (experimentally and computationally the slower route). The experimental and computational estimates of the TS energy barrier for the critical pathway are 14.6 and 16.6 kcal/mol, respectively, while the corresponding TS energy barriers for the bridging hydride isomerization are 20.1 and 21.0 kcal/mol, respectively.[16] Thus, the calculations are in complete accord with the experimental results. It is unexpected that **1D** protonates terminally and so much more rapidly than **1A**, and then rearranges to **2A**, the species that would have been produced by direct protonation of **1A** at the bridging site. It would be interesting to examine this system at lower temperatures by rapid spectroscopic techniques to attempt the detection of terminal hydride species.

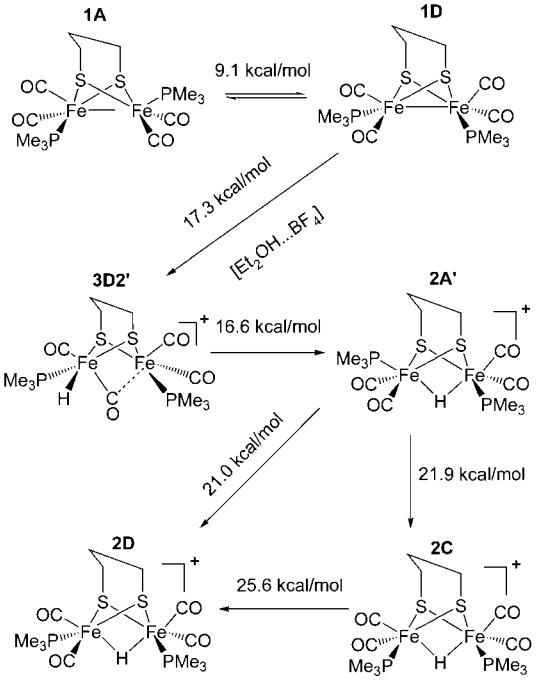

Scheme 4. The most favourable pathways for the bridging-hydride isomers, $Fe_2(\mu\text{-}H)(\mu\text{-}pdt)(CO)_4(PMe_3)_2$, the solvent-corrected free-energy barriers are presented and given in kcal/mol.

Recently, Zampella et al. reported on the isomerization of the terminal- to bridging-hydride in three related diiron cluster models with the edt (ethylenedithiolate) linker.[17] In agreement with our results, the lowest barrier isomerization from terminal hydride to bridging hydride involves the movement of the hydride, the two other ligands on the same iron and the bridging CO via the Ray-Dutt twist. However, once the H is bridging, further rearrangements occur by Bailar twists to the μ-H bonded product.

Computational Details

All calculations have been performed using the Gaussian 03 software package.[18] All DFT calculations were performed using the Becke3LYP (B3LYP) hybrid GGA functional as implemented in Gaussian 03.[19] The geometric structures of all model species were fully optimized as gas phase. The effective core potentials of Hay and Wadt with double-zeta valence basis set (LanL2DZ) was employed to describe iron, phosphorus and sulfur atoms.[20] For iron, the two outermost p functions were replaced by re-optimized 4p functions as suggested by Couty and Hall.[21] Besides, the *f* polarization function was also added in the basis set of Fe.[22a] For sulfur and phosphorus, the basis sets were augmented with the *d* polarization functions proposed by Höllwarth et al.[22b] The 6-31++G** basis set was used for other atoms. At the same level of theory, the Harmonic vibrational frequency calculations were carried out to identify all of the stationary points (zero imaginary frequency) and transition state structures (only one imaginary frequency) and to provide the free energies at T = 298.15 K. And all transition states were confirmed to connect the reactants and products by the intrinsic reaction coordinate (IRC) calculations. Based upon the gas-phase-optimized structures, the effect of solvent was evaluated by single-point calculations using the integral equation formalism polarizable continuum model (IEFPCM) in MeCN in combination with the united atom topological model for the radii setting (RADII = UAHF). The 3D molecular structures displayed in this paper were drawn by using the JIMP2 program.[23] In this paper, the relative free energies in solution were used to analyze the reaction mechanisms.

Supporting Information (see footnote on the first page of this article): Evaluation of density functionals, plots for the optimized structures of the ether-mediated intermediates and transition states for the terminal-path, and the Cartesian coordinates of optimized structures.

Acknowledgments

We acknowledge the financial support of the National Science Foundation (NSF) (CHE-0518074, CHE-0541587, and CHE-0910552) and The Welch Foundation (grant number A-0648).

[1] a) C. Tard, C. J. Pickett, *Chem. Rev.* **2009**, *109*, 2245–2274; b) P. E. M. Siegbahn, J. W. Tye, M. B. Hall, *Chem. Rev.* **2007**, *107*, 4414–4435; c) J. W. Tye, M. B. Hall, M. Y. Darensbourg, *Proc. Natl. Acad. Sci. USA* **2005**, *102*, 16911–16912.

[2] a) M. W. W. Adams, *Biochim. Biophys. Acta Bioenerg. Biochim. Biophys. Acta* **1990**, *1020*, 115–145; b) S. P. J. Albract, *Biochim. Biophys. Acta Bioenerg. Biochim. Biophys. Acta* **1994**, *1188*, 167–204; c) E. Garcin, X. Vernede, E. C. Hatchikian, A. Volbeda, M. Frey, J. C. Fontecilla-Camps, *Structure* **1999**, *7*, 557–566; d) M. Korbas, S. Vogt, W. Meyer-Klaucke, E. Bill, E. J.

Lyon, R. K. Thauer, S. Shima, *J. Biol. Chem.* **2006**, *281*, 30804–30813; e) X. Z. Yang, M. B. Hall, *J. Am. Chem. Soc.* **2009**, *131*, 10901–10908.

[3] a) S. J. Borg, S. K. Ibrahim, C. J. Pickett, S. P. Best, *C. R. Chim.* **2008**, *11*, 852–860; b) A. I. Stewart, I. P. Clark, M. Towrie, S. K. Ibrahim, A. W. Parker, C. J. Pickett, N. T. Hunt, *J. Phys. Chem. B* **2008**, *112*, 10023–10032; c) J. A. Wright, C. J. Pickett, *Chem. Commun.* **2009**, 5719–5721; d) A. Jablonskytė, J. A. Wright, C. J. Pickett, *Dalton Trans.* **2010**, *39*, 3026–3034.

[4] a) X. Zhao, I. P. Georgakaki, M. L. Miller, J. C. Yarbrough, M. Y. Darensbourg, *J. Am. Chem. Soc.* **2001**, *123*, 9710–9711; b) D. Chong, I. P. Georgakaki, R. Mejia-Rodriguez, J. Sanabria-Chinchilla, M. P. Soriaga, M. Y. Darensbourg, *Dalton Trans.* **2003**, 4158–4163; c) C. M. Thomas, O. Rüdiger, T. B. Liu, C. E. Carson, M. B. Hall, M. Y. Darensbourg, *Organometallics* **2007**, *26*, 3976–3984; d) C. M. Thomas, T. B. Liu, M. B. Hall, M. Y. Darensbourg, *Inorg. Chem.* **2008**, *47*, 7009–7024; e) M. L. Singleton, N. Bhuvanesh, J. H. Reibenspies, M. Y. Darensbourg, *Angew. Chem.* **2008**, *120*, 9634; *Angew. Chem. Int. Ed.* **2008**, *47*, 9492–9495.

[5] a) J.-F. Capon, S. El Hassnaoui, F. Gloaguen, P. Schollhammer, J. Talarmin, *Organometallics* **2005**, *24*, 2020–2022; b) S. Ezzaher, J.-F. Capon, F. Gloaguen, F. Y. Pétillon, P. Schollhammer, J. Talarmin, *Inorg. Chem.* **2007**, *46*, 3426–3428; c) . S. Ezzaher, J.-F. Capon, F. Gloaguen, N. Kervarec, F. Y. Pétillon, R. Pichon, P. Schollhammer, J. Talarmin, *C. R. Chim.* **2008**, *11*, 906–914; d) J.-F. Capon, F. Gloaguen, F. Y. Pétillon, P. Schollhammer, J. Talarmin, *Eur. J. Inorg. Chem.* **2008**, 4671–4681; e) J.-F. Capon, S. Ezzaher, F. Gloaguen, F. Y. Pétillon, P. Schollhammer, J. Talarmin, *Chem. Eur. J.* **2008**, *14*, 1954–1964.

[6] a) F. Gloaguen, J. D. Lawrence, T. B. Rauchfuss, *J. Am. Chem. Soc.* **2001**, *123*, 9476–9477; b) A. K. Justice, T. B. Rauchfuss, S. R. Wilson, *Angew. Chem.* **2007**, *119*, 6264; *Angew. Chem. Int. Ed.* **2007**, *46*, 6152–6154; c) M. T. Olsen, M. Bruschi, L. De Gioia, T. B. Rauchfuss, S. R. Wilson, *J. Am. Chem. Soc.* **2008**, *130*, 12021–12030; d) A. K. Justice, M. J. Nilges, T. B. Rauchfuss, S. R. Wilson, L. De Gioia, G. Zampella, *J. Am. Chem. Soc.* **2008**, *130*, 5293–5301; e) Z. M. Heiden, G. Zampella, L. De Gioia, T. B. Rauchfuss, *Angew. Chem.* **2008**, *120*, 9902; *Angew. Chem. Int. Ed.* **2008**, *47*, 9756–9759.

[7] a) M. H. Cheah, S. J. Borg, M. I. Bondin, S. P. Best, *Inorg. Chem.* **2004**, *43*, 5635–5644; b) S. J. Borg, T. Behrsing, S. P. Best, M. Razavet, X. M. Liu, C. J. Pickett, *J. Am. Chem. Soc.* **2004**, *126*, 16988–16999; c) M. H. Cheah, S. J. Borg, S. P. Best, *Inorg. Chem.* **2007**, *46*, 1741–1750; d) M. H. Cheah, C. Tard, S. J. Borg, X. M. Liu, S. K. Ibrahim, C. J. Pickett, S. P. Best, *J. Am. Chem. Soc.* **2007**, *129*, 11085–11092.

[8] a) X. Zhao, Y.-M. Hsiao, C.-H. Lai, J. H. Reibenspies, M. Y. Darensbourg, *Inorg. Chem.* **2002**, *41*, 699–708; b) X. Zhao, I. P. Georgakaki, M. L. Miller, R. Mejia-Rodriguez, C.-Y. Chiang, M. Y. Darensbourg, *Inorg. Chem.* **2002**, *41*, 3917–3928; c) P. I. Volkers, T. B. Rauchfuss, *J. Inorg. Biochem.* **2007**, *101*, 1748–1751.

[9] a) J. I. van der Vlugt, T. B. Rauchfuss, C. M. Whaley, S. R. Wilson, *J. Am. Chem. Soc.* **2005**, *127*, 16012–16013; b) D. Morvan, J.-F. Capon, F. Gloaguen, A. Le Goff, M. Marchivie, F. Michaud, P. Schollhammer, J. Talarmin, J.-J. Yaouanc, *Organometallics* **2007**, *26*, 2042–2052; c) P.-Y. Orain, J.-F. Capon, N. Kervarec, F. Gloaguen, F. Pétillon, R. Pichon, P. Schollhammer, J. Talarmin, *Dalton Trans.* **2007**, 3754–3756; d) B. E. Barton, T. B. Rauchfuss, *Inorg. Chem.* **2008**, *47*, 2261–2263.

[10] a) J. W. Tye, M. Y. Darensbourg, M. B. Hall, *THEOCHEM* **2006**, *771*, 123–128; b) J. A. Franz, S.-J. Lee, T. A. Bowden, M. S. Alnajjar, A. M. Appel, J. C. Birnbaum, T. E. Bitterwolf, M. Dupuis, *J. Am. Chem. Soc.* **2009**, *131*, 15212–15224.

[11] a) B. E. Barton, M. T. Olsen, T. B. Rauchfuss, *J. Am. Chem. Soc.* **2008**, *130*, 16834–16835; b) D. Morvan, J.-F. Capon, F. Gloaguen, F. Y. Pétillon, P. Schollhammer, J. Talarmin, J.-J. Yaouanc, F. Michaud, N. Kervarec, *J. Organomet. Chem.* **2009**, *694*, 2801–2807; c) B. E. Barton, G. Zampella, A. K. Justice, L. De Gioia, T. B. Rauchfuss, S. R. Wilson, *Dalton Trans.* **2010**, *39*, 3011–3019.

[12] a) J. W. Peters, W. N. Lanzilotta, B. J. Lemon, L. C. Seefeldt, *Science* **1998**, *282*, 1853–1858; b) Y. Nicolet, C. Piras, P. Legrand, C. E. Hatchikian, J. C. Fontecilla-Camps, *Structure* **1999**, *7*, 13–23; c) Y. Nicolet, A. L. de Lacey, X. Vernède, V. M. Fernandez, E. C. Hatchikian, J. C. Fontecilla-Camps, *J. Am. Chem. Soc.* **2001**, *123*, 1596–1601.

[13] a) G. Zampella, P. Fantucci, L. De Gioia, *J. Am. Chem. Soc.* **2009**, *131*, 10909–10917; b) P.-Y. Orain, J.-F. Capon, F. Gloaguen, F. Y. Pétillon, P. Schollhammer, J. Talarmin, G. Zampella, L. De Gioia, T. Roisnel, *Inorg. Chem.* **2010**, *49*, 5003–5008.

[14] P. Surawatanawong, M. B. Hall, *Inorg. Chem.* **2010**, *49*, 5737–5747.

[15] S. J. Borg, J. W. Tye, M. B. Hall, S. P. Best, *Inorg. Chem.* **2007**, *46*, 384–394.

[16] J. A. Wright, L. Webster, A. Jablonskytė, P. M. Woi, S. K. Ibrahim, C. J. Pickett, *Faraday Discuss.* **2011**, *148*, 359–371.

[17] G. Zampella, P. Fantucci, L. De Gioia, *Chem. Commun.* **2010**, *46*, 8824–8826.

[18] M. J. Frisch, G. W. Trucks, H. B. Schlegel, G. E. Scuseria, M. A. Robb, J. R. Cheeseman, J. A. Montgomery, Jr., T. Vreven, K. N. Kudin, J. C. Burant, J. M. Millam, S. S. Iyengar, J. Tomasi, V. Barone, B. Mennucci, M. Cossi, G. Scalmani, N. Rega, G. A. Petersson, H. Nakatsuji, M. Hada, M. Ehara, K. Toyota, R. Fukuda, J. Hasegawa, M. Ishida, T. Nakajima, Y. Honda, O. Kitao, H. Nakai, M. Klene, X. Li, J. E. Knox, H. P. Hratchian, J. B. Cross, V. Bakken, C. Adamo, J. Jaramillo, R. Gomperts, R. E. Stratmann, O. Yazyev, A. J. Austin, R. Cammi, C. Pomelli, J. W. Ochterski, P. Y. Ayala, K. Morokuma, G. A. Voth, P. Salvador, J. J. Dannenberg, V. G. Zakrzewski, S. Dapprich, A. D. Daniels, M. C. Strain, O. Farkas, D. K. Malick, A. D. Rabuck, K. Raghavachari, J. B. Foresman, J. V. Ortiz, Q. Cui, A. G. Baboul, S. Clifford, J. Cioslowski, B. B. Stefanov, G. Liu, A. Liashenko, P. Piskorz, I. Komaromi, R. L. Martin, D. J. Fox, T. Keith, M. A. Al-Laham, C. Y. Peng, A. Nanayakkara, M. Challacombe, P. M. W. Gill, B. Johnson, W. Chen, M. W. Wong, C. Gonzalez, J. A. Pople, *Gaussian 03*, revision E.01, Gaussian, Inc., Wallingford, CT, **2004**.

[19] a) A. D. Becke, *J. Chem. Phys.* **1993**, *98*, 5648–5652; b) C. Lee, W. Yang, R. G. Parr, *Phys. Rev.* **1988**, *37*, 785–789; c) B. Miehlich, A. Savin, H. Stoll, H. Preuss, *Chem. Phys. Lett.* **1989**, *157*, 200–206.

[20] a) P. J. Hay, W. R. Wadt, *J. Chem. Phys.* **1985**, *82*, 284–298; b) P. J. Hay, W. R. Wadt, *J. Chem. Phys.* **1985**, *82*, 270–283; c) P. J. Hay, W. R. Wadt, *J. Chem. Phys.* **1985**, *82*, 299–310.

[21] M. Couty, M. B. Hall, *J. Comput. Chem.* **1996**, *17*, 1359–1370.

[22] a) A. W. Ehlers, M. Biihme, S. Dapprich, A. Gobbi, A. Hijllwarth, V. Jonas, K. F. Kiihler, R. Stegmann, A. Veldkamp, G. Frenking, *Chem. Phys. Lett.* **1993**, *208*, 111–114; b) A. Höllwarth, M. Biihme, S. Dapprich, A. W. Ehlers, A. Gobbi, V. Jonas, K. F. Köhler, R. Stegmann, A. Veldkamp, G. Frenking, *Chem. Phys. Lett.* **1993**, *208*, 237–240.

[23] a) J. Manson, C. E. Webster, M. B. Hall, *JIMP2, a free program for Visualizing and manipulating molecules*, version 0.091, Texas A&M University, College Station, TX, **2006**; b) M. B. Hall, R. F. Fenske, *Inorg. Chem.* **1972**, *11*, 768–775.

Received: October 12, 2010
Published Online: January 26, 2011

